The N-Terminal Peptides of the Three Human Isoforms of the Mitochondrial Voltage-Dependent Anion Channel Have Different Helical Propensities

ARTICLE *in* BIOCHEMISTRY · AUGUST 2015

Impact Factor: 3.02 · DOI: 10.1021/acs.biochem.5b00469 · Source: PubMed

8 AUTHORS, INCLUDING:

Mariano Andrea Scorciapino

Università degli studi di Cagliari

50 PUBLICATIONS **327** CITATIONS

SEE PROFILE

Vito De Pinto

University of Catania

58 PUBLICATIONS **1,598** CITATIONS

SEE PROFILE

Matteo Ceccarelli

Università degli studi di Cagliari

86 PUBLICATIONS **1,419** CITATIONS

SEE PROFILE

Mariano Casu

Università degli studi di Cagliari

142 PUBLICATIONS **2,000** CITATIONS

SEE PROFILE

BIOCHEMISTRY
including biophysical chemistry & molecular biology

Article

pubs.acs.org/biochemistry

The N-Terminal Peptides of the Three Human Isoforms of the Mitochondrial Voltage-Dependent Anion Channel Have Different Helical Propensities

Carlo Guardiani,[†] Mariano Andrea Scorciapino,[*,‡,§] Giuseppe Federico Amodeo,[∥] Joze Grdadolnik,[⊥] Giuseppe Pappalardo,[#] Vito De Pinto,[@] Matteo Ceccarelli,[†,§] and Mariano Casu[∥]

[†]Department of Physics, University of Cagliari, 09042 Monserrato, Italy

[‡]Department of Biomedical Sciences, Biochemistry Unit, University of Cagliari, 09042 Monserrato, Italy

[§]Istituto Officina dei Materiali del Consiglio Nazionale delle Ricerche (IOM-CNR), UOS, Cagliari, Italy

[∥]Department of Chemical and Geological Sciences, University of Cagliari, 09042 Monserrato, Italy

[⊥]National Institute of Chemistry, Ljubljana, Slovenia

[#]CNR Institute of Biostructures and Bioimaging, Catania, Italy

[@]Department of Biological, Geological and Environmental Sciences, Section of Molecular Biology, University of Catania, and National Institute for Biostructures and Biosystems, Section of Catania, Catania, Italy

Supporting Information

ABSTRACT: The voltage-dependent anion channel (VDAC) is the main mitochondrial porin allowing the exchange of ions and metabolites between the cytosol and the mitochondrion. In addition, VDAC was found to actively interact with proteins playing a fundamental role in the regulation of apoptosis and being of central interest in cancer research. VDAC is a large transmembrane β-barrel channel, whose N-terminal helical fragment adheres to the channel interior, partially closing the pore. This fragment is considered to play a key role in protein stability and function as well as in the interaction with apoptosis-related proteins. Three VDAC isoforms are differently expressed in higher eukaryotes, for which distinct and complementary roles are proposed. In this work, the folding propensity of their N-terminal fragments has been compared. By using multiple spectroscopic techniques, and complementing the experimental results with theoretical computer-assisted approaches, we have characterized their conformational equilibrium. Significant differences were found in the intrinsic helical propensity of the three peptides, decreasing in the following order: hVDAC2 > hVDAC3 > hVDAC1. In light of the models proposed in the literature to explain voltage gating, selectivity, and permeability, as well as interactions with functionally related proteins, our results suggest that the different chemicophysical properties of the N-terminal domain are possibly correlated to different functions for the three isoforms. The overall emerging picture is that a similar transmembrane water accessible conduit has been equipped with not identical domains, whose differences can modulate the functional roles of the three VDAC isoforms.

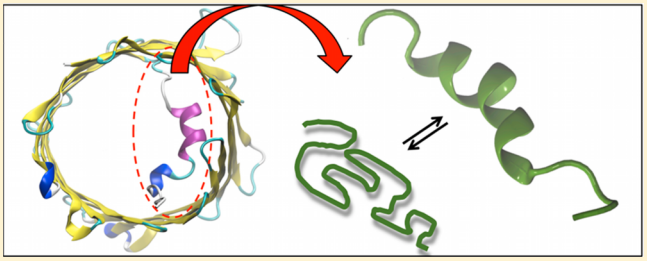

The voltage-dependent anion channel (VDAC) is a 30 kDa pore-forming protein mainly located in the outer mitochondrial membrane (OMM). Its main function is to form a general pore for ions and small metabolites, among which the energetic nucleotides ATP, ADP, and NADH are particularly important. VDAC is anion selective in the open state, but it switches to a partially closed state when the applied transmembrane voltage is increased above 30−40 mV, with the closed state characterized by a reduced permeability and slight cation selectivity.[1−4] In addition to guaranteeing the exchange of ions and metabolites between the cytosol and the mitochondrion, VDAC has been found to actively interact with other proteins like hexokinase[5] and Bcl-2 family members,[6] playing a fundamental role in the regulation of pathways related to apoptosis[7,8] and cancer.[9,10] Three different VDAC isoforms are expressed in higher eukaryotes. Among the three, VDAC1 is the most abundant, being 10 and 100 times more prevalent than VDAC2 and VDAC3, respectively, in the majority of cells.[3,11,12]

VDAC is a large transmembrane channel (outer diameter of 4.5 nm, inner diameter of 2.0−2.5 or 3.0 nm with the N-terminal domain inside or outside, respectively, and height of 4 nm) formed by 19 β-strands arranged in a regular antiparallel organization, whereas the parallel pairing of strands 1 and 19 completes the β-barrel.[13−16] Both the N- and C-termini face the mitochondrial intermembrane space.[17] The most evident

Received: April 28, 2015
Revised: August 22, 2015
Published: August 24, 2015

DOI: 10.1021/acs.biochem.5b00469
Biochemistry 2015, 54, 5646−5656

difference among the three human isoforms is the longer N-terminal fragment of hVDAC2, which has 11 more residues than the other two isoforms (Figure 1). The N-terminal

```
                          1   5    10   15   20   25
hVDAC1(1-25)    ----------MAVPPTYADLGKSARDVFTKGYGFG
hVDAC2(1-36)    MATHGQTCARPMCIPPSYADLGKAARDIFNKGFGFG
hVDAC3(1-25)    ----------MCNTPTYCDLGKAAKDVFNKGYGFG
                          *. .*:*.****:*:*:*.**:***
```

Figure 1. Multiple-sequence alignment of the N-terminal fragment of the three isoforms of hVDAC. Residues are numbered according to hVDAC1 and hVDAC3 sequence; thus, the first 11 residues of hVDAC2 are not numbered in the figure (asterisks denote identity, colons a high degree of similarity, and periods a low degree of similarity).

fragment of VDAC (the first 25 amino acid residues, 36 in the case of hVDAC2) is located inside the lumen, partially closing the pore. However, differences exist between the available three-dimensional (3D) structures, and they mainly refer to the N-terminal portion itself.[13−16] In human[15] and mouse[14] VDAC1, as well as in zebrafish VDAC2,[16] the N-terminal fragment crosses the channel and presents a helical fold from residue 6 to 20. In the structure reported by Hiller et al.,[13] despite being termed human VDAC1 as in Bayrhuber et al.,[15] the same protein fragment is characterized by a mostly unfolded conformation. Basically, a well-folded N-terminal fragment was observed through X-ray crystallography[14−16] [in the case of Bayrhuber et al.[15] a hybrid X-ray/nuclear magnetic resonance (NMR) approach was applied]. On the other hand, NMR showed that at room temperature in the liquid state, thus better reflecting cell conditions, the N-terminal domain most probably exists as an ensemble of conformations with a remarkable fraction of unfolded states.[13]

This N-terminal domain is considered to play a key role in both protein stability and functionality. It is crucial for stabilization of the open state and in voltage gating,[18−23] as well as for the interaction with apoptosis-related proteins.[3,8,9,24] hVDAC1 has no cysteine residues, whereas both hVDAC2 and hVDAC3 are characterized by the presence of two cysteines in the N-terminal region. It is not known whether they form disulfide bridges with other cysteines located in the barrel wall, but this should deeply affect the N-terminal mobility and, in turn, the specific isoform functioning.

In light of these differences and the different expression levels of the three human isoforms of VDAC, the possibility of distinct and complementary roles has been put forward.[11,12] In the work presented here, the folding propensity of the N-terminal peptides of the three hVDACs was compared, focusing on the aligned portion (Figure 1). By using both experimental and theoretical approaches, their conformational plasticity has been characterized in a physiological buffer, to highlight possible differences in their intrinsic behavior. The effects of the presence of physiologically relevant electrolytes were also investigated. This is a fundamental step for further biophysical studies aimed at characterizing the interaction between such an important fragment of VDAC and any of the proteins involved in its biochemical functions. Knowledge of the intrinsic features, a sort of N-terminal peptide's fingerprint, is the basis for understanding what is actually caused by the interaction and the interacting counterpart(s), toward the unveiling of the functional differences among the three isoforms.

MATERIALS AND METHODS

Materials. Synthetic peptides were purchased from Peptide Protein Research Ltd. (Fareham, U.K.) with a purity of 98% and with the C-terminus amidated. In particular, hVDAC1(1−25) (MAVPPTYADLGKSARDVFTKGYGFG), hVDAC2(12−36) (MCIPPSYADLGKAARDIFNKGFGFG), and hVDAC3(1−25) (MCNTPTYCDLGKAAKDVFNKGYGFG) were investigated. The 3-(trimethylsilyl)-2,2′,3,3′-tetradeuteropropionic acid (TSP) was purchased from Cambridge Isotope Laboratories (Andover, MA). All other chemicals were supplied by Sigma-Aldrich. Peptides were dissolved in 10 mM phosphate buffer (PB; pH 7.4). In the case of hVDAC2(12−36) and hVDAC3(1−25), because of the presence of cysteine residues in the amino acid sequence, the reducing agent 1,4-dithio-D-threitol (DTT) was added at a 1:3 peptide:DTT molar ratio, to prevent the formation of disulfide bridges.

Circular Dichroism (CD) Spectroscopy. CD spectra of the three peptides (20 μM) were recorded on a Jasco J-810 spectropolarimeter with a 1 mm path length cell. Spectra were recorded in the spectral range of 190−260 nm, with a scan rate of 10 nm/min at 0.1 nm intervals. Data were acquired at 300 K, and 10 scans were averaged for each spectrum. Peptide CD spectra were collected either in 10 mM PB or in the presence of additional electrolytes to investigate the effect of physiologically relevant counterions on the peptide intrinsic folding propensity. In particular, either Na^+ or K^+ ions were added to the PB at a final concentration of 100 mM, to test the effect of a large excess of these monovalent cations, matching a typical physiological condition. Also, the presence of Mg^{2+} ions was checked but keeping the Mg:peptide molar ratio to 1:1. Cations were added to the PB as dibasic sulfate salts. Despite chlorides being more physiologically relevant anions, they strongly absorb below 195 nm and are therefore not recommended for CD investigations.[25]

Attenuated Total Reflectance Infrared Spectroscopy (ATR-IR). Spectra were recorded on liquid-state samples (10 μL) at room temperature with a Bruker Vector 22 spectrometer equipped with a diamond single-reflection ATR accessory (Platinum ATR module) and a liquid N_2-cooled MCT detector. Spectra were acquired in the range of 4000−600 cm^{-1} (4 cm^{-1} spectral resolution) and are an average of 256 scans. The peptide concentration was 7 mM. For each sample, water evaporation was followed, in addition, by recording a spectrum every 5 min until no further spectral changes were observed. On average, 40 min was necessary to get almost complete water evaporation and obtain a spectrum of the solid film formed on the surface of the diamond. The formation of the solid film significantly improved the signal:noise ratio and band resolution. ATR-IR spectra of peptides were recorded in 10 mM PB in the presence of additional electrolytes. In particular, either Na^+, K^+, or Mg^{2+} ions were added to a final concentration of 100, 100, or 7 mM, respectively. Cations were added to the PB as chloride salts. The full width at half-maximum (fwhm) was estimated by fitting the amide I band with a single Gaussian function. No band deconvolution to quantify different components was attempted.

Nuclear Magnetic Resonance (NMR). Peptides were dissolved in PB at a concentration of 2 mM. The pH was corrected to 5.0 with small aliquots of 0.1 M HCl to minimize the backbone amide protons exchange rate with water.[26] Spectra were recorded with an Agilent Unity Inova 500NB instrument operating at a ^1H frequency of 500 MHz.

DOI: 10.1021/acs.biochem.5b00469
Biochemistry 2015, 54, 5646−5656

Experiments were conducted at 300 K. The chemical shift scale of either ^{1}H and ^{13}C was referenced to the methyl signal of TSP (2 mM). ^{1}H spectra were recorded using a 6.6 μs pulse (90°), a 1 s delay time, a 2 s acquisition time, and a 7 kHz spectral width. Suppression of the water signal was achieved through the application of the WET sequence[27,28] (the uburp shape was centered at the water resonance with a width of 100 Hz). ^{1}H−^{1}H DQF-COSY experiments were conducted over the same spectral window using 2048 complex points and sampling each of the 512 increments with 64 scans. The same acquisition parameters have been applied, together with a mixing time of 80 ms (MLEV-17 spin-lock scheme), for the acquisition of TOCSY spectra. The NOESY experiments were conducted with the same acquisition parameters and a mixing time of either 200 or 250 ms. The ^{1}H−^{13}C HSQC spectra were recorded using spectral windows of 7 and 21 kHz for ^{1}H and ^{13}C, respectively, and sampling each of the 512 increments with 64 scans. The $^3J_{HNH\alpha}$ coupling constants were measured from DQF-COSY spectra. The chemical shift values of ^{1}Hα, ^{1}Hβ, ^{13}Cα, and ^{13}Cβ were analyzed with TALOS+[29] in comparison to its high-resolution structural database.

Bioinformatics Analyses. The polarity score for amino acids was calculated through the ExPASy web portal, available at http://expasy.org/. The method of Grantham has been applied[30] over windows of three residues and rescaling by 50% the score of the window edges. The helical propensity was estimated with the predictive algorithm Agadir[31−35] at a temperature of 300 K, an ionic strength of 0.1 M, and pH 7.4.

Molecular Dynamics (MD) Simulations. Simulations started with the peptide in the fully extended conformation, embedded in a truncated octahedral simulation box comprising ∼10000 water molecules. Sodium and chloride ions have been added to the systems to neutralize the peptide net charge and produce a final NaCl concentration of 10 mM. All simulations were performed with Amber14[36] using the ff14SB force field and the TIP3P water model. To avoid possible entrapment in metastable minima, the enhanced sampling technique Hamiltonian Replica Exchange MD (H-REMD)[37,38] was employed.

In the classical temperature REMD,[39] a number of system replicas are simulated in parallel at different temperatures. Exchanges between neighboring replicas are attempted at regular time intervals, which are accepted or rejected according to a Metropolis-like probability:

$$p_{ij} = \min\{1, \exp[-(\beta_i - \beta_j)(E_j - E_i)]\} \quad (1)$$

where E_i and E_j are the energies of the replicas involved and β_i and β_j are their inverse temperatures. For bulky molecular systems, the large ΔE imposes a rather small $\Delta\beta$ to attain sufficiently high exchange rates, resulting in an increase in the number of replicas and, thus, the computational cost.

This can be avoided in H-REMD, where replicas have different Hamiltonians, or energy functions, and exchanges are attempted between adjacent Hamiltonians with an acceptance probability:

$$p_{ij} = \min\{1, \exp\{-\beta_1[E_1(x_2) - E_1(x_1)] - \beta_2[E_2(x_1) - E_2(x_2)]\}\} \quad (2)$$

In this work, all replicas were run at the same temperature and the energy function of the ith replica was $E_i = E_{nt} + \lambda_i E_t$, where E_t is the torsional energy of the backbone dihedral angles and E_{nt} lumps together all the other energy terms. By substitution into eq 2, the E_{nt} contributions cancel out, so that exchange acceptance probability depends only on the torsional term:

$$p_{ij} = \min\{1, \exp\{-\beta(\lambda_1 - \lambda_2)[E_t(x_2) - E_t(x_1)]\}\} \quad (3)$$

Following Bergonzo et al.,[40] the dihedral force constants were all uniformly scaled by a constant factor, from 1.0 (full force field) to 0.3 in intervals of 0.1, leading to eight replicas. Each replicas first underwent 1000 steps of steepest descent minimization followed by 1000 steps of conjugate gradient minimization. Replicas were then equilibrated for 5 ns in the *NVT* ensemble using a time step of 2 fs and a temperature of 300 K with the Langevin thermostat. The last frame was used as input for the subsequent H-REMD simulation. Each replica was run for 100 ns attempting exchanges every 2.5 ps (acceptance probability in the range of 55−65%).

The secondary structure analysis of the trajectory with full torsional force (λ = 1.0) was performed using the DSSP algorithm.[41] CD spectra were calculated on the basis of the MD trajectories as a linear combination of experimental reference spectra for purely α-helix, β-sheet, and random-coil conformations, where the weighting factors[a] are the frequencies obtained from the DSSP analysis.[42,43]

RESULTS

Circular Dichroism Spectroscopy. The CD spectra obtained for the three peptides in PB are shown in Figure 2.

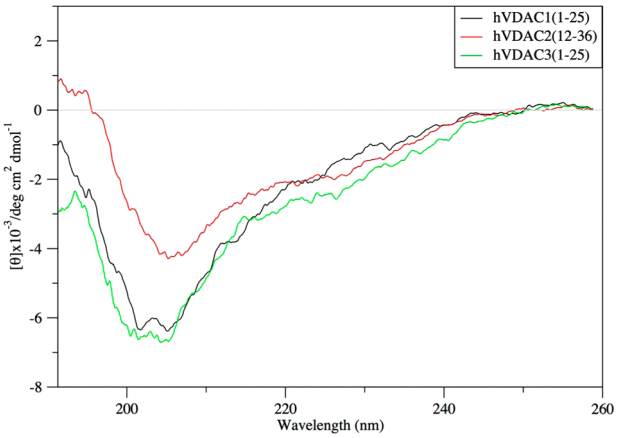

Figure 2. CD spectra of N-terminal peptides of hVDACs. Spectra recorded in phosphate buffer (10 mM, pH 7.4) are shown with the ordinate reporting the mean residue ellipticity.

Spectra of hVDAC1(1−25) and hVDAC3(1−25) show a similar spectral shape, with a main broad negative band at a wavelength significantly higher than 200 nm, and negative ellipticity in the range of 190−195 nm. The presence of an additional band around 220 nm cannot be ruled out. Despite a random-coil conformation perhaps being inferred at first glance, these spectral features are not compatible either with a polyproline helix or with a purely random-coil conformation. On the other hand, the spectrum of hVDAC2(12−36) is remarkably different. The main negative band is characterized by a lower ellipticity and is shifted toward a higher wavelength, while slightly positive ellipticity is observed in the range of 190−195 nm. Moreover, the presence of at least one additional negative band around 220 nm is evident in this case. Two different states contribute to the spectrum: the "random coil",

DOI: 10.1021/acs.biochem.5b00469
Biochemistry 2015, 54, 5646−5656

with its negative ellipticity at 200 nm, and the "α-helix", with two negative bands at 208 and 222 nm and a positive one at 192 nm, which partially cancels out the random-coil negative band on the shortest wavelength side (Figure 2).

The influence of different cations, namely, Na^+, K^+, and Mg^{2+}, was also investigated. Figure 3 shows the CD spectra

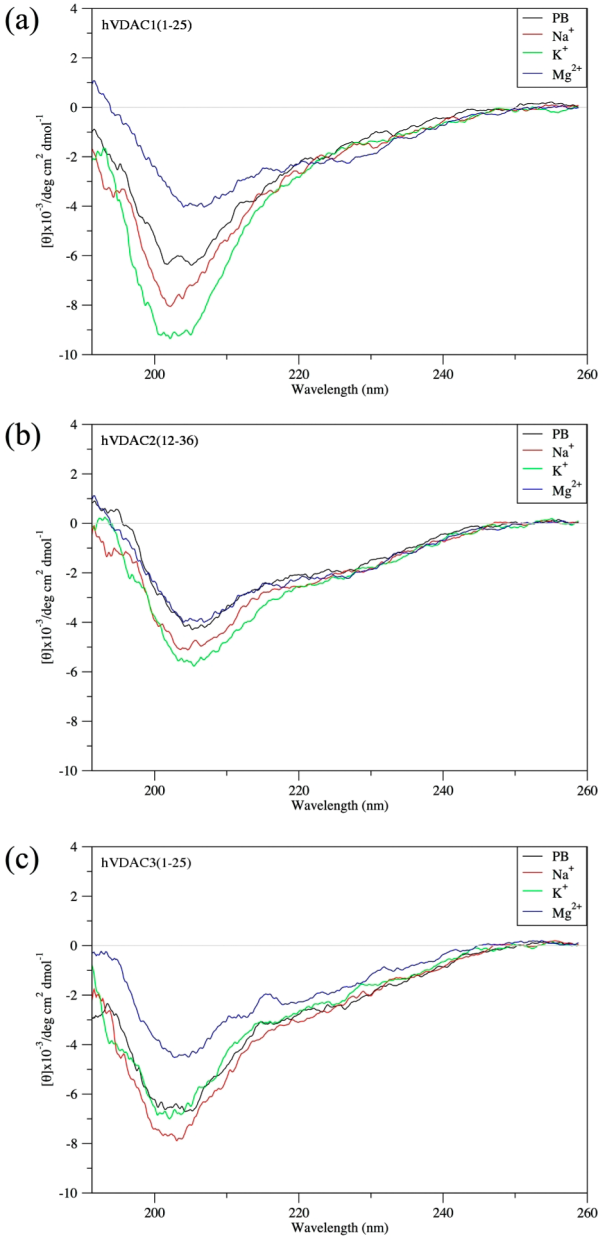

Figure 3. Effect of cations on CD spectra of N-terminal peptides of hVDACs. Spectra recorded in the presence of Na^+, K^+, or Mg^{2+} in phosphate buffer (10 mM, pH 7.4) are shown for (a) hVDAC1(1−25), (b) hVDAC2(12−36), and (c) hVDAC3(1−25). The corresponding spectrum obtained in the buffer (Figure 2) is also shown for direct comparison.

acquired from the three peptides in the presence of the different metal ions added to the PB. No dramatic differences were observed in the spectral shape or in the band position, indicating that, under our experimental conditions, the influence of such cations on the conformational equilibrium was negligible for each of the three peptides under investigation. However, in the presence of 1 equiv of Mg^{2+}, the spectrum of both hVDAC1(1−25) and hVDAC3(1−25) was similar to those obtained for hVDAC2(12−36).

Infrared (IR) Spectroscopy. IR spectra were recorded in ATR mode for both the liquid-state samples and the corresponding solid film. The latter were always characterized by a significantly higher signal:noise ratio and band resolution. Figure 4 shows, for instance, the liquid and the film spectra of

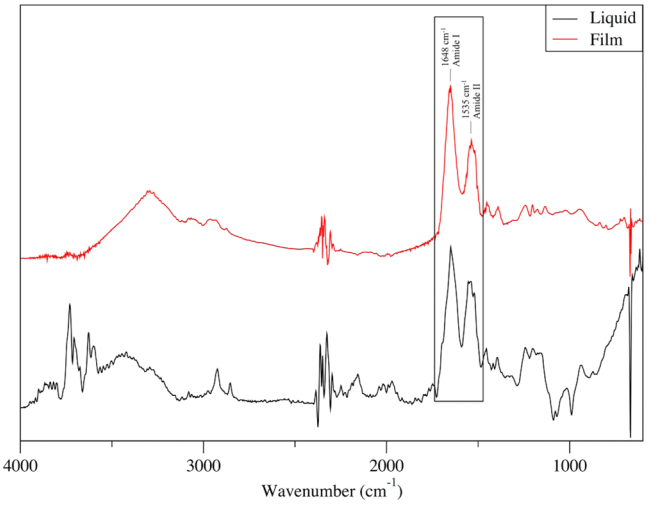

Figure 4. Comparison of liquid and film IR spectra. ATR-IR spectrum of hVDAC1(1−25) in phosphate buffer (10 mM, pH 7.4) recorded for the sample in the liquid state and the corresponding solid film.

hVDAC1(1−25) in PB. The position of the maximum of the amide I band and its fwhm in the absence and presence of different cations in the PB are reported in Table 1.

In the liquid state, the amide I band was always broader than in the film, which is indicative of multiple conformations. In the film spectra, the band position was consistently found to be that typical of helical folding. However, while both hVDAC2(12−36) and hVDAC3(1−25) reached a value of 1654 cm^{-1} (and a fwhm of ∼50 cm^{-1}), hVDAC1(1−25) exhibits slightly a red-shifted amide I maximum centered at 1648 cm^{-1} with a broader fwhm (61 cm^{-1}), suggesting a less regular and/or a bent helical fold.[44] In the liquid state, a general wavenumber decrease was observed as usual for water-exposed disordered helices.[44]

The presence of the different cations added to the PB, namely, Na^+, K^+, and Mg^{2+}, did not result in a significant shift (spectral resolution of 4 cm^{-1}) of the amide I band in all the studied cases, both for the solution and for the solid film spectra. This indicates that, under our experimental conditions, their influence on the peptide conformational equilibrium was negligible.

Nuclear Magnetic Resonance Spectroscopy. The N-terminal peptide of the three human isoforms of VDAC was investigated in PB. The ^1H and ^{13}C resonances were assigned on the basis of a set of two-dimensional experiments, namely, DQF-COSY, TOCSY, NOESY, and $^1H-^{13}C$ HSQC, as described by Cavanagh et al.[26] Results are reported in Tables S1−S3 for hVDAC1(1−25), hVDAC2(12−36), and hVDAC3(1−25), respectively. The chemical shift index (CSI) values were calculated for both the α-protons and α-carbons;[45−47] however, deviations from the reference "random coil" values were negligible, and in general, no peptide portions with specific CSI values were identified, indicating the absence

DOI: 10.1021/acs.biochem.5b00469
Biochemistry 2015, 54, 5646−5656

Table 1. Infrared Amide I Band Positions and Widths for the N-Terminal Peptide of hVDACs (7 mM) in the Absence and Presence of Different Cations in Phosphate Buffer (spectral resolution of 4 cm^{-1})

	wavenumber (fwhm) (cm^{-1})			
film spectra	PB[a]	Na^{+}[b]	K^{+}[b]	Mg^{2+}[c]
hVDAC1(1−25)	1648 (61)	1648 (60)	1648 (62)	1648 (61)
hVDAC2(12−36)	1653 (52)	1653 (53)	1654 (52)	1654 (50)
hVDAC3(1−25)	1653 (52)	1656 (48)	1650 (52)	1654 (51)
	wavenumber (fwhm) (cm^{-1})			
liquid spectra	PB[a]	Na^{+}[b]	K^{+}[b]	Mg^{2+}[c]
hVDAC1(1−25)	1644 (63)	1642 (76)	1642 (82)	1644 (69)
hVDAC2(12−36)	1646 (71)	1639 (77)	1647 (71)	1649 (59)
hVDAC3(1−25)	1652 (87)	–[d] (–)	1648 (60)	1649 (55)

[a]In 10 mM phosphate buffer (pH 7.4). [b]At 100 mM. [c]At 7 mM. [d]The band was clearly multicomponent.

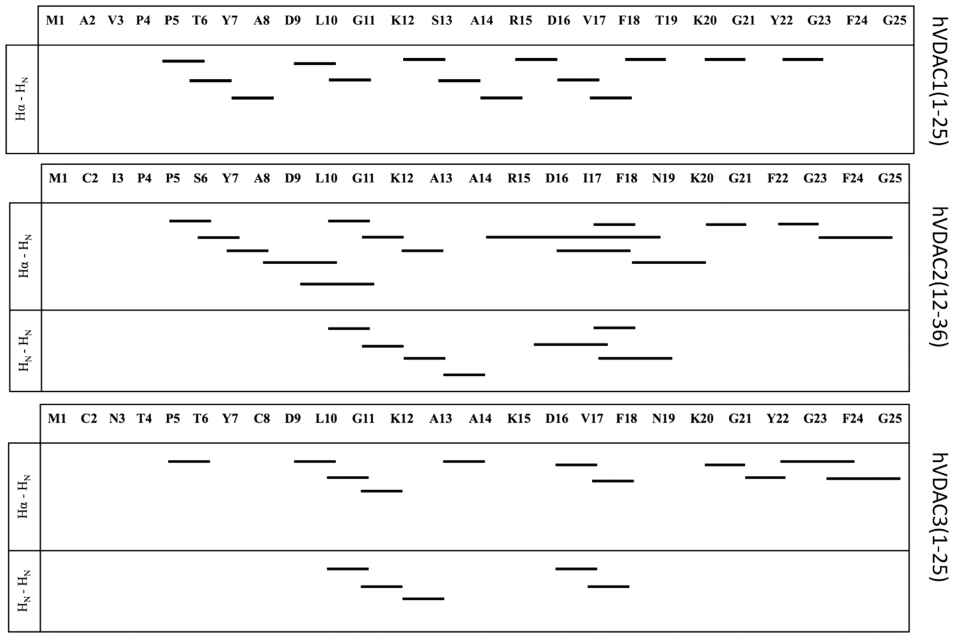

Figure 5. Sequential interproton NOEs. Proton−proton dipolar interactions found for hVDAC1(1−25), hVDAC2(12−36), and hVDAC3(1−25) in 10 mM phosphate buffer are reported as lines connecting the two residues involved.

of any well-defined folded structure. The experimental chemical shift values of $^{1}H\alpha$, $^{1}H\beta$, $^{13}C\alpha$, and $^{13}C\beta$ were also analyzed via TALOS+[29] in comparison to its high-resolution structural database. In agreement with the CSI analysis, the majority of residues were either classified as "ambiguous" (meaning that no specific secondary structure could be predicted with sufficient confidence) or recognized as part of highly dynamic portions of the peptide. The very few predictions ranked as "good" were sparse along the peptide sequence such that a reliable secondary structure prediction was not possible. Nevertheless, it was quite interesting to find that the only exception was a cluster of three consecutive residues in hVDAC2(12−36), namely, K23, A24, and A25. These residues are located exactly in the middle of the peptide sequence, and their backbone conformation was estimated as being helical with a very high consensus. In agreement, all the measured $^{3}J_{HNH\alpha}$ scalar coupling constants were found in the range of 6−8 Hz, reflecting motional averaging of multiple conformations,[26] but those of hVDAC2(12−36) A24 and A25, which were 3.5 Hz, typical of helical conformations.

Some differences among the three peptides were also observed in the dipolar through-space sequential correlations. Figure 5 schematically shows the observed sequential $^{1}H-^{1}H$ NOESY cross-peaks (NOEs). A different number of NOEs were observed for the three peptides under investigation, increasing in the following order: hVDAC1(1−25) < hVDAC3(1−25) < hVDAC2(12−36). In the case of hVDAC1(1−25), only short-range HN−Hα (i, i + 1) NOEs were identified. Several short-range HN−HN (i, i + 1) NOEs were assigned, in addition, in the case of hVDAC3(1−25). Finally, hVDAC2(12−36) was characterized by a significantly higher number of NOEs. Both sequential HN−Hα and HN−HN NOEs were found, some short-range and several medium-range.

Bioinformatics Analyses. The polarity score profile (Figure 6a) shows that the more and less polar residues are alternated along the amino acid sequence. The pattern is absolutely comparable for the three hVDAC N-terminal peptides, the largest differences being found only at the very beginning of the sequence. The application of the Agadir algorithm resulted in a rather low helix probability in PB (Figure 6b), with the three peptides sharing the same range of residues with a non-zero probability, i.e., 6−20. Despite the

DOI: 10.1021/acs.biochem.5b00469
Biochemistry 2015, 54, 5646−5656

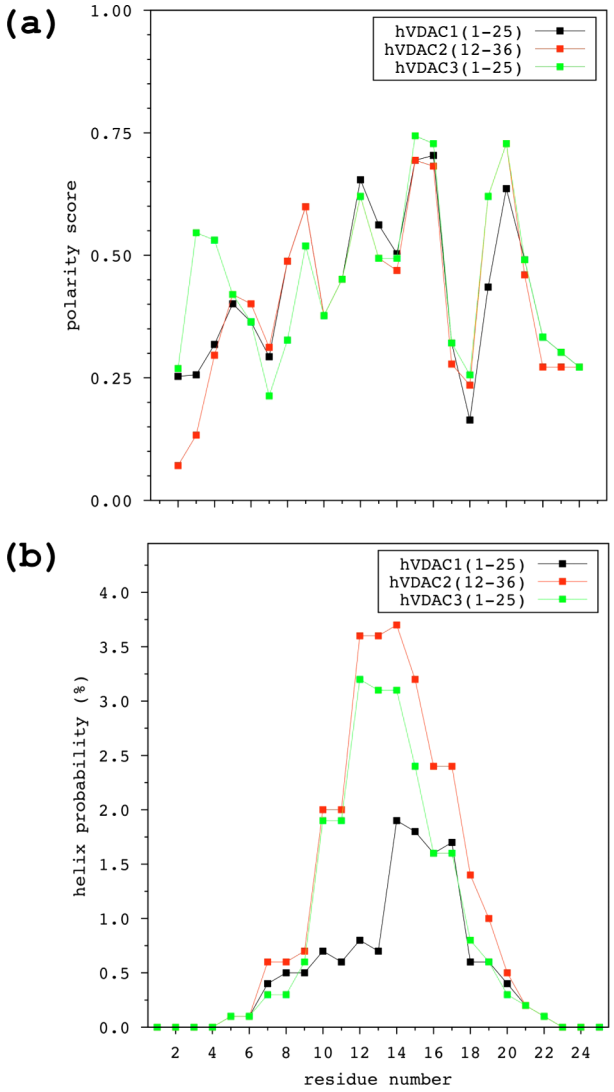

Figure 6. Bioinformatics analyses. The polarity score is shown in panel a for the three peptides as a function of residue number. The higher the score, the more polar the amino acid residue. Agadir prediction (300 K, pH 7.4, ionic strength of 0.1 M) is shown in panel b as the helix percentage as a function of residue number.

values being low, the trend hVDAC2(12−36) > hVDAC3(1−25) > hVDAC1(1−25) is evident.

Molecular Dynamics Simulations. Peptide secondary structure analysis was performed on the target replica using the DSSP algorithm.[41] This is based on the assignment of the backbone hydrogen bonding pattern to different secondary structure motifs, namely, α-, π-, and 3_{10}-helix, parallel and antiparallel β-strand, and β-turn. Figure 7 shows the frequency of these secondary structure elements along the amino acid sequence of the three peptides under investigation. Although the "random coil" was the prevalent state for all three hVDAC peptides, a significant occurrence of α-helix, 3_{10}-helix, and β-turn was revealed. While in both hVDAC1(1−25) and hVDAC3(1−25) the α-helix shows a profile with two peaks, one around the eighth and the second around the 16th residue, hVDAC2(12−36) is characterized by a single wide peak in the α-helix profile. Such a single peak has the maximum located around the 16th residue but covers the same range spanned by the distribution obtained for the other two peptides, without any breakage (Figure 7d). On the other hand, the 3_{10}-helix profiles are comparable for the three peptides (Figure 7b), with an asymmetric bimodal distribution where the peak on the N-terminus side is the most populated. Results are summarized in Table 2, where the helical propensity ranking hVDAC2(12−36) ≥ hVDAC3(1−25) > hVDAC1(1−25) is clear.

These data were used to reconstruct the CD spectra of the three hVDAC peptides (Figure 8). All the calculated CD spectra are characterized by a main negative band at a wavelength slightly higher than 200 nm. An additional negative band is present around 220 nm, which is more pronounced in the case of hVDAC2(12−36) but clearly detectable also in the spectra of both hVDAC1(1−25) and hVDAC3(1−25). In the latter cases, negative ellipticity was obtained in the range of 190−195 nm and slightly positive for hVDAC2(12−36). Interestingly, when one moves along the series of hVDAC1(1−25), hVDAC3(1−25), and hVDAC2(12−36), the more intense the negative band at ∼220 nm, the more the main band at ∼200 nm shifts to higher wavelength values and the more its intensity decreases. By considering that the β-type structure contribution was negligible in the reconstruction of the CD spectra, which was almost completely caused by a different proportion of helical and random-coil fraction, we can conclude that calculated spectra reflect the different helical contents of the three peptides: hVDAC2(12−36) > hVDAC3-(1−25) > hVDAC1(1−25).

DISCUSSION

The spectra recorded in PB for both hVDAC1(1−25) and hVDAC3(1−25) are very similar to those reported in the literature for the hVDAC1(2−20) peptide.[48] Despite random-coil conformation usually being observed for relatively short polypeptides, unless a suitable folding−promoting cosolvent or a lipid membrane model is present,[48−51] a closer inspection of the CD spectra suggests that the peptide exists in equilibrium between completely random-coil states and partially folded states characterized by helical fragments of variable length. The case of hVDAC2(12−36) is even more clear. The CD spectrum results from two different contributions: the "random-coil" and "α-helix" conformation. The same also applies to hVDAC1(1−25) and hVDAC3(1−25), but the proportion of "random coil" is higher.

All three hVDAC peptides resulted in mostly unfolded forms in PB; however, the existing equilibrium with a helical folding was clearly seen, and in particular, the intrinsic helical propensity is higher for hVDAC2(12−36). When K^+, Na^+, or Mg^{2+} was added to the buffer, CD spectra did not show any dramatic change (Figure 3), clearly indicating that the helical propensity of hVDAC peptides is not affected by these physiologically relevant ions. The slight differences and, in particular, the fact that a relatively low concentration of Mg^{2+} was sufficient to make the spectra of hVDAC1(1−25) and hVDAC3(1−25) comparable to those obtained for hVDAC2(12−36) are certainly interesting and suggest ion-specific effects on folding equilibria[52] but would require specific investigations and are beyond the scope of this work.

In PB, the IR amide I bands of the three hVDAC peptides were rather broad (Table 1), presumably because of the overlap of multiple conformations, confirming the predominant random-coil state in solution. Addition of different electrolytes to the buffer supported the CD results that indicated a negligible effect on the conformational equilibrium in solution, although differences in the bandwidth suggest subtle ion-specific effects. Moving from solution to solid film spectra,

DOI: 10.1021/acs.biochem.5b00469
Biochemistry 2015, 54, 5646−5656

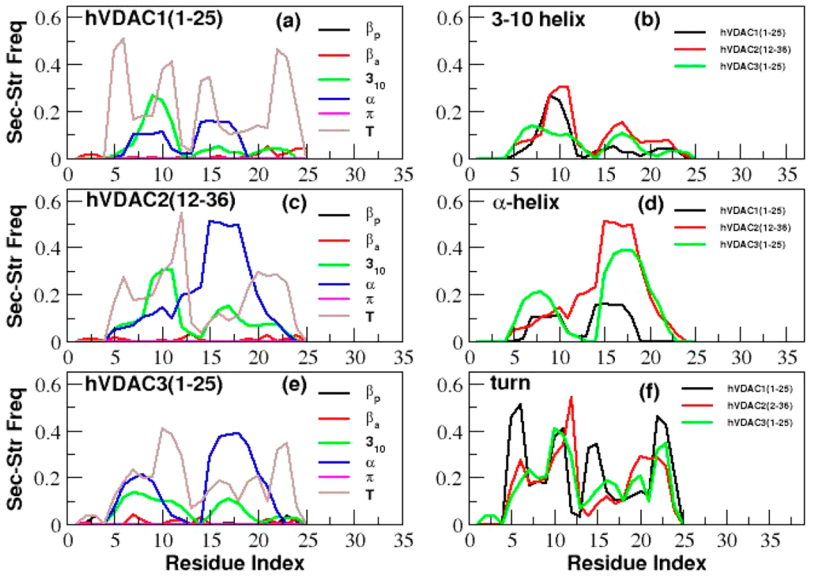

Figure 7. Secondary structure profile obtained for the N-terminal peptides of the three hVDAC isoforms. Panels a, c, and e show the frequency of all the investigated secondary structure motifs for hVDAC1(1−25), hVDAC2(12−36), and hVDAC3(1−25), respectively (β_p, parallel β-strand; β_a, antiparallel β-strand; 3_{10}, 3_{10}-helix; α, α-helix; π, π-helix; T, β-turn). In panels b, d, and f, the three peptides are directly compared with respect to the profiles of 3_{10}-helix, α-helix, and β-turn, respectively.

Table 2. Secondary Structure Content[a] of the N-Terminal Peptide of hVDACs Calculated by the DSSP Analysis of the MD Trajectory

motif	hVDAC1(1−25)	hVDAC2(12−36)	hVDAC3(1−25)
random coil	0.69	0.58	0.64
α-helix	0.05	0.16	0.13
3_{10}-helix	0.05	0.08	0.05
π-helix	<0.01	<0.01	<0.01
β-parallel	<0.01	<0.01	<0.01
β-antiparallel	0.01	<0.01	<0.01
β-turn	0.19	0.16	0.16

[a]The fraction of a given secondary structure is obtained by normalizing to 1 the sum of all the residues of all the frames found to be involved in that secondary structure motif.

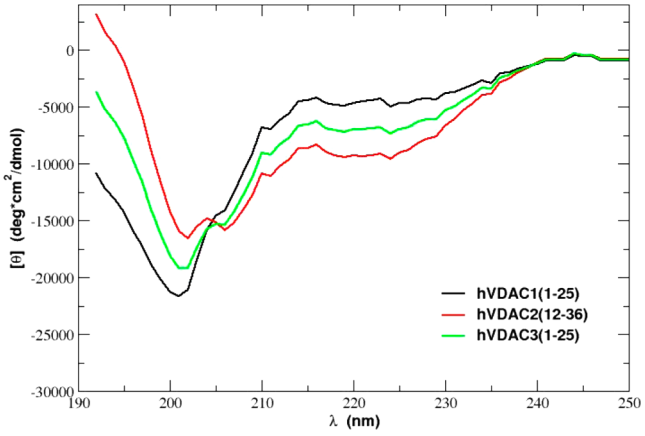

Figure 8. Calculated CD spectra of the N-terminal peptides of the three hVDAC isoforms. Reconstruction of spectra has been performed on the basis of the conformations visited along the trajectory of the target replica of the H-REMD simulation.

peptides assumed a more rigid conformation upon dehydration and consequent adhesion to the diamond surface of the ATR device. Despite the band position being consistently found to be that typical of helical folding in all cases, a slightly lower wavenumber and a higher bandwidth were found for hVDAC1(1−25), suggesting a less regular and/or a bent helical folding.[44]

The analysis of ^{1}H and ^{13}C NMR chemical shifts, the lack of significant deviations from the "random coil" reference values,[45−47] the $^3J_{HNHa}$ coupling constants in the range of 6−8 Hz, and the small number of NOEs observed in all cases clearly indicate that all three N-terminal hVDAC peptides adopted highly dynamical conformations in PB. However, the number of NOEs (Figure 5) followed the order hVDAC1(1−25) < hVDAC3(1−25) < hVDAC2(12−36), with the latter being the only case in which some medium-range interactions were observed, suggesting a slight but significant difference in the conformational equilibrium. Actually, only in the case of hVDAC2(12−36) did we find three consecutive residues (K23, A24, and A25) having their chemical shift values compatible with a helical conformation, with two of them (A24 and A25) showing a $^3J_{HNHa}$ coupling constant of 3.5 Hz, typical for helices. Nevertheless, for the sake of clarity, it has to be stressed that the 3D structure could not be determined in any case, because the number of NMR parameters was too small and motional averaging evident from our results.

Results from three independent techniques supported each other and, despite all hVDAC peptides being mostly random coil in solution, a slight but significant difference among the three was consistently found. CD indicated that hVDAC2(12−36) has the highest helical propensity. IR suggested hVDAC1(1−25) as the one with the less regular structure upon dehydration. NMR supported the same trend of folding propensity: hVDAC2(12−36) > hVDAC3(1−25) > hVDAC1(1−25). It has to be noted that NMR experiments were performed at pH 5.0 to minimize the backbone amide proton exchange rate with the solvent, whereas the other techniques were employed at the physiological pH of 7.4. However, no significant differences are expected between these two pH values in the case presented here. The three amino acid

DOI: 10.1021/acs.biochem.5b00469
Biochemistry 2015, 54, 5646−5656

sequences have no histidine residues, and the protonation state of all the residues (calculated with PropKa[53]) does not change significantly in the pH range of 5.0−7.4.

Helical propensity predictions by the software Agadir[31−35] are in perfect agreement with this trend (Figure 6). The overall helical propensity is low for each of the peptides, but this is not surprising considering that predictions are performed without taking into account the presence of any possible support for folding, like a lipid membrane model or a folding−promoting cosolvent. It is also very interesting to note that the range of non-zero helical propensity, residues 6−20, is in very good agreement with the folded portion observed in whole protein simulations.[54]

The secondary structure analysis performed on the H-REMD simulations (used instead of classical MD to avoid the drawback of the system being trapped in a metastable minimum and thus sampling only a limited region of the phase space) further confirmed that the three hVDAC peptides have a significant intrinsic helical content. In agreement with the experimental results, computer simulations revealed a clear ranking of helicity: hVDAC2(12−36) > hVDAC3(1−25) > hVDAC1(1−25). In particular, the secondary structure profile of both 3_{10}- and α-helical conformations turned out to be highly asymmetric for all the hVDAC peptides (Figure 7b,d), with the highest values in the residue index ranges of 6−12 and 13−20, respectively. This specific segregation of the 3_{10}- and α-contribution to the overall helicity is in very good agreement with the secondary structure profile obtained for the three peptides when simulated as part of the entire hVDAC channels.[54] This bimodal profile is also in remarkable agreement with the discontinuous nature of the N-terminal domain in different crystal structures available in the Protein Data Bank (PDB), namely, in mouse VDAC1 (PDB entry 3EMN)[14] and zebrafish VDAC2 (PDB entry 4BUM).[16] The calculated CD spectra (Figure 8), finally, are in excellent qualitative agreement with the experimental spectra (Figure 2), bolstering the different equilibrium between random-coil and helical states for the three hVDAC N-terminal peptides.

In the VDAC structure,[14−16] the N-terminal fragment folds back into the lumen and adheres to the barrel wall approximately at the midpoint of the hydrophobic portion of the membrane. It forms a restricted zone, which defines the size exclusion limit for the permeation of molecules and largely determines the electrostatic potential inside the lumen,[21,54] deeply affecting ions and metabolites selectivity. However, the exact localization of the N-terminal fragment differs among the available 3D structures of VDAC1,[13−15] leading to different hypotheses about the mechanism of voltage gating.[18−20,54,55] Unbinding of the N-terminal fragment from the channel wall is involved in most of the models, with this fragment remaining inside the lumen, moving out to the cytosol or even binding to the external leaflet of the OMM.[8,9,18,19] In addition, the exposition of the N-terminal peptide outside the channel has been shown in several reports,[56] and the N-terminal peptide, indeed, was shown to be absolutely essential for the interaction of VDAC with anti-apoptotic proteins like hexokinase and Bcl2.[9,24]

When bound to the channel wall, the folded state is stabilized by two main factors: (i) helix amphipathicity[54] and (ii) specific hydrogen bonds and hydrophobic contacts.[13−15,54] The amino acid sequence is such that the helical folded conformation turns out to be highly amphipathic (Figure 6a) and is thus favored by the interaction with a suitable surface such that the hydrophilic side will be solvent-exposed, while the hydrophobic one will be protected from water contacts. Indeed, our ATR-IR results have shown that helical folding is enhanced upon dehydration and film formation, because of adhesion of the peptide on the diamond surface. Such "surface-assisted" folding was previously observed for hVDAC1(2−20) upon interaction with detergent micelles[48] and for hVDAC1(2−17) with liposomes.[57] Upon unbinding, on the other hand, the folded peptide will be progressively more exposed to water, and on the basis of the work presented here, it is expected to tend toward a mostly random-coil state. This conclusion is supported by the NMR 3D structure of the entire hVDAC1,[13] in contrast to the hybrid crystallographic/NMR structure in which the N-terminal peptide appears to be well folded and attached on the barrel β-strands.[15]

In the literature, a sequence-specific prefolding equilibrium has been postulated for peptides in aqueous solution and characterized through computational approaches.[51,58,59] Before interacting with a suitable surface or in the absence of any folding promoting cosolvent (e.g., trifluoroethanol), however, the random-coil states are so largely populated with respect to the folded states that such an equilibrium is extremely hard to be capture by experiments that include CD, IR, or NMR spectroscopy at room temperature. This work reveals that, despite the high level of sequence homology shared by the N-terminal fragment of the three human VDAC isoforms, their helical propensity follows the order hVDAC2(12−36) > hVDAC3(1−25) > hVDAC1(1−25). This specific trend agrees with recently published MD simulations performed on the whole hVDAC isoforms,[54] where the N-terminal fragment although located inside the lumen and bound to the β-barrel, showed a different conformational plasticity for this important protein domain, with hVDAC1 being the one with the highest mobility.

A different helical propensity might translate into a different unbound and unfolded−bound and folded equilibrium, because the more stable the helical fold, the more hindered the N-terminal fragment unbinding from the channel wall, possibly affecting the channel behavior.[b] The different helical propensity shown here pertains to the N-terminal peptides alone, such that findings cannot be straightforwardly transferred to the intact proteins, especially concerning its detailed mechanism. Nevertheless, it is very interesting to note further correlations from the literature.

In a recent straightforward experiment, indeed, two residues (R15 and D16 in rat VDAC1) in the N-terminal fragment were mutated to proline.[60] This residue was employed as a helix breaker, resulting in the increase in the random-coil conformation propensity accompanied by unbinding from the barrel and possible exposure outside the pore lumen.[60] Such mutagenized VDAC1 showed a specific asymmetric voltage dependence upon reconstitution in a planar lipid bilayer: at high negative voltages, the slope of the conductance ratio G/G_0 decreases,[60] indicative of a weakened ability of the pore to gate. These observations are complemented by the functional analysis of another mutagenized pore: the large deletion of β-hairpin 9−10, where the main actors in the hydrophobic contacts stabilizing N-terminal helix−β-barrel interaction, V143 an L150, are located,[61] produced a fully asymmetric voltage dependence of the hVDAC.[62]

It might be also suggested that the random-coil state of the unbound N-terminal domain could represent the key for the interaction with hexokinase and Bcl2 family proteins through a

DOI: 10.1021/acs.biochem.5b00469
Biochemistry 2015, 54, 5646−5656

"conformational selection" process.[63] Different conformations are in thermal equilibrium with each other, and the most favored is selected upon binding, which would also provide a possible explanation for the same domain being able to interact with different proteins.

The three human isoforms of VDAC have different expression levels (depending also on the specific tissue), and a number of pieces of evidence that bolster possible different and complementary roles have been collected.[11,12] In light of the importance of the N-terminal fragment for the numerous VDAC activities,[9,13−15,18−20,24,54,55] it is possible that different roles for the three isoforms might be due, at least in part, to the different chemicophysical properties of their N-terminal fragment. In this regard, the work by Reina et al.[64] is particularly interesting, where the swapping of the N-terminal domain between the different isoforms resulted in a dramatic alteration of the channel functionality. In this work, we have introduced a comparative investigation showing intrinsic similarity and dissimilarity among the three N-terminal fragment of hVDAC isoforms. The overall emerging picture is that a similar but not identical domain has been equipped with subtle differences. Whether such differences directly or indirectly contribute to the modulation of the functional roles of the three human VDAC isoforms remains to be unveiled but certainly deserves further attention with more specific and tailored approaches.

■ ASSOCIATED CONTENT

Supporting Information

The Supporting Information is available free of charge on the ACS Publications website at DOI: 10.1021/acs.biochem.5b00469.

NMR resonance assignments (PDF)

■ AUTHOR INFORMATION

Corresponding Author

*Department of Biomedical Sciences, Biochemistry Unit, University of Cagliari, Cittadella Universitaria di Monserrato-S.P. 8, km 0.700, 09042 Monserrato (CA), Italy. Telephone: +39-070-675-3921. Fax: +39-070-675-4527. E-mail: scorciapino@unica.it.

Funding

This work was supported by the Italian Ministero dell'Istruzione, dell'Università e della Ricerca, MIUR (PRIN Project 2010CSJX4F and FIRB-MERIT Project RBNE08HWLZ). Regione Autonoma della Sardegna, RAS, is also greatly acknowledged for the visiting professors program (decision n. 56/21). J.G. acknowledges the Regione Autonoma della Sardegna (RAS decision n. 56/21) for sponsoring the visiting professor grant he enjoyed at the University of Cagliari.

Notes

The authors declare no competing financial interest.

■ ABBREVIATIONS

ATR, attenuated total reflectance; CD, circular dichroism; CSI, chemical shift index; DTT, 1,4-dithio-D-threitol; fwhm, full width at half-maximum; H-REMD, Hamiltonian replica exchange molecular dynamics; MD, molecular dynamics; OMM, outer mitochondrial membrane; PB, phosphate buffer; PDB, Protein Data Bank; TSP, 3-(trimethylsilyl)-2,2′,3,3′-tetradeuteropropionic acid; VDAC, voltage-dependent anion channel.

■ ADDITIONAL NOTES

[a]The number of secondary structure types included in the DSSP analysis (α-, π-, and 3_{10}-helix, parallel and antiparallel β-strand, β-turn, and random coil) is larger than the number of reference spectra used for CD spectrum calculation (α-helix, β-sheet, and random coil). Thus, the contributions of α-, π-, and 3_{10}-helix have been summed up to yield the single fraction of helical conformation. Similarly, contributions of parallel and antiparallel β-strands have been merged together with β-turn content to produce a single fraction of β-type conformation. [b]For the sake of completeness, it has to be mentioned that the major difference in the amino acid sequences of the three N-terminal peptides is the presence of two cysteine residues only in hVDAC2 and hVDAC3. The position of only one of the two cysteines is conserved. It is not known if disulfide bridges are formed with other cysteine residues located in the β-barrel, which would certainly lead to important differences in the mobility of the N-terminal fragment. Moreover, hVDAC2 has 11 N-terminal residues more than the other two isoforms, which were neglected in this work to focus on the behavior of the segment shared by all the human isoforms.

■ REFERENCES

(1) Benz, R. (1994) Permeation of hydrophilic solutes through mitochondrial outer membranes: review on mitochondrial porins. *Biochim. Biophys. Acta, Rev. Biomembr. 1197*, 167−196.

(2) Colombini, M. (2004) VDAC: the channel at the interface between mitochondria and the cytosol. *Mol. Cell. Biochem. 256−257*, 107−115.

(3) Shoshan-Barmatz, V., De Pinto, V., Zweckstetter, M., Raviv, Z., Keinan, N., and Arbel, N. (2010) VDAC, a multi-functional mitochondrial protein regulating cell life and death. *Mol. Aspects Med. 31*, 227−285.

(4) Rostovtseva, T., and Colombini, M. (1997) VDAC channels mediate and gate the flow of ATP: implications for the regulation of mitochondrial function. *Biophys. J. 72*, 1954−1962.

(5) Beutner, G., Ruck, A., Riede, B., and Brdiczka, D. (1997) Complexes between hexokinase, mitochondrial porin and adenylate translocator in brain: regulation of hexokinase, oxidative phosphorylation and permeability transition pore. *Biochem. Soc. Trans. 25*, 151−157.

(6) Cheng, E. H. Y., Sheiko, T. V., Fisher, J. K., Craigen, W. J., and Korsmeyer, S. J. (2003) VDAC2 inhibits BAK activation and mitochondrial apoptosis. *Science 301*, 513−517.

(7) Tomasello, F. M., Messina, A., Lartigue, L., Schembri, L., Medina, C., Reina, S., Thoraval, D., Crouzet, M., Ichas, F., De Pinto, V., and De Giorgi, F. (2009) Outer membrane VDAC1 controls permeability transition of the inner mitochondrial membrane in cellulo during stress-induced apoptosis. *Cell Res. 19*, 1363−1376.

(8) Shoshan-Barmatz, V., Keinan, N., Abu-Hamad, S., Tyomkin, D., and Aram, L. (2010) Apoptosis is regulated by the VDAC1 N-terminal region and by VDAC oligomerization: release of cytochrome c, AIF and Smac/Diablo. *Biochim. Biophys. Acta, Bioenerg. 1797*, 1281−1291.

(9) Shoshan-Barmatz, V., and Ben-Hail, D. (2012) VDAC, a multi-functional mitochondrial protein as a pharmacological target. *Mitochondrion 12*, 24−34.

(10) Maldonado, E. N., and Lemasters, J. J. (2012) Warburg revisited: regulation of mitochondrial metabolism by voltage-dependent anion channels in cancer cells. *J. Pharmacol. Exp. Ther. 342*, 637−641.

(11) Messina, A., Reina, S., Guarino, F., and De Pinto, V. (2012) VDAC isoforms in mammals. *Biochim. Biophys. Acta, Biomembr. 1818*, 1466−1476.

(12) De Pinto, V., Guarino, F., Guarnera, A., Messina, A., Reina, S., Tomasello, F. M., Palermo, V., and Mazzoni, C. (2010) Character-

DOI: 10.1021/acs.biochem.5b00469
Biochemistry 2015, 54, 5646−5656

ization of human VDAC isoforms: a peculiar function for VDAC3? *Biochim. Biophys. Acta, Bioenerg. 1797*, 1268−1275.
(13) Hiller, S., Garces, R. G., Malia, T. J., Orekhov, V. Y., Colombini, M., and Wagner, G. (2008) Solution structure of the integral human membrane protein VDAC-1 in detergent micelles. *Science 321*, 1206−1210.
(14) Ujwal, R., Cascio, D., Colletier, J.-P., Faham, S., Zhang, J., Toro, L., Ping, P., and Abramson, J. (2008) The crystal structure of mouse VDAC1 at 2.3 A resolution reveals mechanistic insights into metabolite gating. *Proc. Natl. Acad. Sci. U. S. A. 105*, 17742−17747.
(15) Bayrhuber, M., Meins, T., Habeck, M., Becker, S., Giller, K., Villinger, S., Vonrhein, C., Griesinger, C., Zweckstetter, M., and Zeth, K. (2008) Structure of the human voltage-dependent anion channel. *Proc. Natl. Acad. Sci. U. S. A. 105*, 15370−15375.
(16) Schredelseker, J., Paz, A., López, C. J., Altenbach, C., Leung, C. S., Drexler, M. K., Chen, J.-N., Hubbell, W. L., and Abramson, J. (2014) High resolution structure and double electron-electron resonance of the zebrafish voltage-dependent anion channel 2 reveal an oligomeric population. *J. Biol. Chem. 289*, 12566−12577.
(17) Tomasello, F. M., Guarino, F., Reina, S., Messina, A., and De Pinto, V. (2013) The voltage-dependent anion selective channel 1 (VDAC1) topography in the mitochondrion outer membrane as detected in intact cell. *PLoS One 8*, e81522.
(18) Teijido, O., Ujwal, R., Hillerdal, C.-O., Kullman, L., Rostovtseva, T. K., and Abramson, J. (2012) Affixing N-terminal α-helix to the wall of the voltage-dependent anion channel does not prevent its voltage gating. *J. Biol. Chem. 287*, 11437−11445.
(19) Zachariae, U., Schneider, R., Briones, R., Gattin, Z., Demers, J., Giller, K., Maier, E., Zweckstetter, M., Griesinger, C., Becker, S., Benz, R., de Groot, B. L., and Lange, A. (2012) b-Barrel Mobility Underlies Closure of the Voltage-Dependent Anion Channel. *Structure 20*, 1540−1549.
(20) Rui, H., Lee, K. I., Pastor, R. W., and Im, W. (2011) Molecular dynamics studies of ion permeation in VDAC. *Biophys. J. 100*, 602−610.
(21) Choudhary, O. P., Ujwal, R., Kowallis, W., Coalson, R., Abramson, J., and Grabe, M. (2010) The electrostatics of VDAC: implications for selectivity and gating. *J. Mol. Biol. 396*, 580−592.
(22) Song, J., Midson, C., Blachly-Dyson, E., Forte, M., and Colombini, M. (1998) The sensor regions of VDAC are translocated from within the membrane to the surface during the gating processes. *Biophys. J. 74*, 2926−2944.
(23) Mannella, C. a. (1998) Conformational changes in the mitochondrial channel protein, VDAC, and their functional implications. *J. Struct. Biol. 121*, 207−218.
(24) Abu-Hamad, S., Arbel, N., Calo, D., Arzoine, L., Israelson, A., Keinan, N., Ben-Romano, R., Friedman, O., and Shoshan-Barmatz, V. (2009) The VDAC1 N-terminus is essential both for apoptosis and the protective effect of anti-apoptotic proteins. *J. Cell Sci. 122*, 1906−1916.
(25) Kelly, S. M., and Price, N. C. (2000) The use of circular dichroism in the investigation of protein structure and function. *Curr. Protein Pept. Sci. 1*, 349−384.
(26) Cavanagh, J., Fairbrother, W. J., Palmer, A. G., III, Rance, M., and Skelton, N. J. (2007) *Protein NMR Spectroscopy: Principles and Practice*, 2nd ed., Elsevier Academic Press, Oxford, U.K.
(27) Ogg, R., Kingsley, P., and Taylor, J. (1994) WET, a T1- and B1-Insensitive Water-Suppression Method for in Vivo Localized 1H NMR Spectroscopy. *J. Magn. Reson., Ser. B 104*, 1−10.
(28) Smallcombe, S., Patt, S. L., and Keifer, P. (1995) WET solvent suppression and its applications to LC NMR and high-resolution NMR spectroscopy. *J. Magn. Reson., Ser. A 117*, 295−303.
(29) Shen, Y., Delaglio, F., Cornilescu, G., and Bax, A. (2009) TALOS+: a hybrid method for predicting protein backbone torsion angles from NMR chemical shifts. *J. Biomol. NMR 44*, 213−223.
(30) Grantham, R. (1974) Amino acid difference formula to help explain protein evolution. *Science 185*, 862−864.
(31) Muñoz, V., and Serrano, L. (1994) Elucidating the folding problem of helical peptides using empirical parameters. *Nat. Struct. Biol. 1*, 399−409.
(32) Muñoz, V., and Serrano, L. (1995) Elucidating the folding problem of helical peptides using empirical parameters. II. Helix macrodipole effects and rational modification of the helical content of natural peptides. *J. Mol. Biol. 245*, 275−296.
(33) Muñoz, V., and Serrano, L. (1995) Elucidating the folding problem of helical peptides using empirical parameters. III. Temperature and pH dependence. *J. Mol. Biol. 245*, 297−308.
(34) Muñoz, V., and Serrano, L. (1997) Development of the multiple sequence approximation within the AGADIR model of alpha-helix formation: comparison with Zimm-Bragg and Lifson-Roig formalisms. *Biopolymers 41*, 495−509.
(35) Lacroix, E., Viguera, A. R., and Serrano, L. (1998) Elucidating the folding problem of alpha-helices: local motifs, long-range electrostatics, ionic-strength dependence and prediction of NMR parameters. *J. Mol. Biol. 284*, 173−191.
(36) Case, D. A., Babin, V., Berryman, J. T., Betz, R. M., Cai, Q., Cerutti, D. S., Cheatham, T. E., III, Darden, T. A., Duke, R. E., Gohlke, H., Goetz, A. W., Gusarov, S., Homeyer, N., Janowski, P., Kaus, J., Kolossvary, I., Kovalenko, A., Lee, T. S., LeGrand, S., Luchko, T., Luo, R., Madej, B., Merz, K. M., Paesani, F., Roe, D. R., Roitberg, A., Sagui, C., Salomon-Ferrer, R., Seabra, G., Simmerling, C. L., Smith, W., Swails, J., Walker, R. C., Wang, J., Wolf, R. M., Wu, X., and Kollman, P. A. (2012) *AMBER 14*, University of California, San Francisco.
(37) Fukunishi, H., Watanabe, O., and Takada, S. (2002) On the Hamiltonian replica exchange method for efficient sampling of biomolecular systems: Application to protein structure prediction. *J. Chem. Phys. 116*, 9058−9067.
(38) Kannan, S., and Zacharias, M. (2007) Enhanced sampling of peptide and protein conformations using replica exchange simulations with a peptide backbone biasing-potential. *Proteins: Struct., Funct., Genet. 66*, 697−706.
(39) Sugita, Y., and Okamoto, Y. (1999) Replica-exchange molecular dynamics method for protein folding. *Chem. Phys. Lett. 314*, 141−151.
(40) Bergonzo, C., Henriksen, N. M., Roe, D. R., Swails, J. M., Roitberg, A. E., and Cheatham, T. E. (2014) Multidimensional Replica Exchange Molecular Dynamics Yields a Converged Ensemble of an RNA Tetranucleotide. *J. Chem. Theory Comput. 10*, 492−499.
(41) Kabsch, W., and Sander, C. (1983) Dictionary of Protein Secondary Structure: Pattern Recognition of Hydrogen-Bonded and Geometrical Features. *Biopolymers 22*, 2577−2637.
(42) Sreerama, N., and Woody, R. W. (1993) A self-consistent method for the analysis of protein secondary structure from circular dichroism. *Anal. Biochem. 209*, 32−44.
(43) Greenfield, N. J., and Fasman, G. D. (1969) Computed circular dichroism spectra for the evaluation of protein conformation. *Biochemistry 8*, 4108−4116.
(44) Barth, A. (2007) Infrared spectroscopy of proteins. *Biochim. Biophys. Acta, Bioenerg. 1767*, 1073−1101.
(45) Wishart, D. S., Sykes, B. D., and Richards, F. M. (1991) Relationship between nuclear magnetic resonance chemical shift and protein secondary structure. *J. Mol. Biol. 222*, 311−333.
(46) Wishart, D. S., Sykes, B. D., and Richards, F. M. (1992) The Chemical Shift Index: A Fast and Simple Method for the Assignment of Protein Secondary Structure through NMR Spectroscopy. *Biochemistry 31*, 1647−1651.
(47) Wishart, D. S., and Sykes, B. D. (1994) The 13C Chemical-Shift Index: A Simple Method for the Identification of Protein Secondary Structure Using 13C Chemical-Shift Data. *J. Biomol. NMR 4*, 171−180.
(48) De Pinto, V., Tomasello, F., Messina, A., Guarino, F., Benz, R., La Mendola, D., Magrì, A., Milardi, D., and Pappalardo, G. (2007) Determination of the conformation of the human VDAC1 N-terminal peptide, a protein moiety essential for the functional properties of the pore. *ChemBioChem 8*, 744−756.
(49) Strandberg, E., and Ulrich, A. S. (2004) NMR methods for studying membrane-active antimicrobial peptides. *Concepts Magn. Reson., Part A 23A*, 89−120.
(50) Manzo, G., Sanna, R., Casu, M., Mignogna, G., Mangoni, M. L., Rinaldi, A. C., and Scorciapino, M. A. (2012) Toward an improved

DOI: 10.1021/acs.biochem.5b00469
Biochemistry 2015, 54, 5646−5656

structural model of the frog-skin antimicrobial peptide esculentin-1b(1−18). *Biopolymers 97*, 873−881.
(51) Scorciapino, M. A., Pirri, G., Vargiu, A. V., Ruggerone, P., Giuliani, A., Casu, M., Buerck, J., Wadhwani, P., Ulrich, A. S., and Rinaldi, A. C. (2012) A novel dendrimeric peptide with antimicrobial properties: structure-function analysis of SB056. *Biophys. J. 102*, 1039−1048.
(52) Crevenna, A. H., Naredi-Rainer, N., Lamb, D. C., Wedlich-Söldner, R., and Dzubiella, J. (2012) Effects of Hofmeister Ions on the α-Helical Structure of Proteins. *Biophys. J. 102*, 907−915.
(53) Dolinsky, T. J., Nielsen, J. E., McCammon, J. A., and Baker, N. A. (2004) PDB2PQR: an automated pipeline for the setup of Piosson-Boltzmann electrostatics calculations. *Nucleic Acids Res. 32*, W665−W667.
(54) Amodeo, G. F., Scorciapino, M. A., Messina, A., De Pinto, V., and Ceccarelli, M. (2014) Charged Residues Distribution Modulates Selectivity of the Open State of Human Isoforms of the Voltage Dependent Anion-Selective Channel. *PLoS One 9*, e103879.
(55) Hiller, S., Abramson, J., Mannella, C., Wagner, G., and Zeth, K. (2010) The 3D structures of VDAC represent a native conformation. *Trends Biochem. Sci. 35*, 514−521.
(56) Guo, X. W., Smith, P. R., Cognon, B., D'Arcangelis, D., Dolginova, E., and Mannella, C. A. (1995) Molecular Design of the Voltage-Dependent, Anion-Selective Channel in the Mitochondrial Outer Membrane. *J. Struct. Biol. 114*, 41−59.
(57) Schneider, R., Etzkorn, M., Giller, K., Daebel, V., Eisfeld, J., Zweckstetter, M., Griesinger, C., Becker, S., and Lange, A. (2010) The native conformation of the human VDAC1 N terminus. *Angew. Chem., Int. Ed. 49*, 1882−1885.
(58) D'Abramo, M., Rinaldi, A. C., Bozzi, A., Amadei, A., Mignogna, G., Di Nola, A., and Aschi, M. (2006) Conformational behavior of temporin A and temporin L in aqueous solution: a computational/experimental study. *Biopolymers 81*, 215−224.
(59) Roccatano, D., Colombo, G., Fioroni, M., and Mark, A. E. (2002) Mechanism by which 2,2,2-trifluoroethanol/water mixtures stabilize secondary-structure formation in peptides: A molecular dynamics study. *Proc. Natl. Acad. Sci. U. S. A. 99*, 12179−12184.
(60) Geula, S., Ben-Hail, D., and Shoshan-Barmatz, V. (2012) Structure-based analysis of VDAC1: N-terminus location, translocation, channel gating and association with anti-apoptotic proteins. *Biochem. J. 444*, 475−485.
(61) Villinger, S., Briones, R., Giller, K., Zachariae, U., Lange, A., de Groot, B. L., Griesinger, C., Becker, S., and Zweckstetter, M. (2010) Functional dynamics in the voltage-dependent anion channel. *Proc. Natl. Acad. Sci. U. S. A. 107*, 22546−22551.
(62) Reina, S., Magrì, A., Lolicato, M., Guarino, F., Impellizzeri, A., Maier, E., Benz, R., Ceccarelli, M., De Pinto, V., and Messina, A. (2013) Deletion of b-strands 9 and 10 converts VDAC1 voltage-dependence in an asymmetrical process. *Biochim. Biophys. Acta, Bioenerg. 1827*, 793−805.
(63) Boehr, D. D., Nussinov, R., and Wright, P. E. (2009) The role of dynamic conformational ensembles in biomolecular recognition. *Nat. Chem. Biol. 5*, 789−796.
(64) Reina, S., Palermo, V., Guarnera, A., Guarino, F., Messina, A., Mazzoni, C., and De Pinto, V. (2010) Swapping of the N-terminus of VDAC1 with VDAC3 restores full activity of the channel and confers anti-aging features to the cell. *FEBS Lett. 584*, 2837−2844.

DOI: 10.1021/acs.biochem.5b00469
Biochemistry 2015, 54, 5646−5656